Journal of Sound and Vibration (2002) **257**(3), 477–501
doi:10.1006/jsvi.5049, available online at http://www.idealibrary.com on IDEAL®

INVESTIGATION AND MODELLING OF THE WALL PRESSURE FIELD BENEATH A TURBULENT BOUNDARY LAYER AT LOW AND MEDIUM FREQUENCIES

D. J. J. Leclercq† and X. Bohineust

PSA Peugeot Citroën Direction de la Recherche et de l'Innovation Automobile, Route de Gisy, F-78943 Vélizy-Villacoublay Cedex, France.

(*Received* 23 *August* 2000, *and in final form* 2 *January* 2002)

In the case of a vehicle moving in a fluid, computation of flow-induced panel vibrations, and the resulting sound generated inside the passenger compartment requires a model that describes the statistics of the turbulent wall pressure fluctuations accurately. However, the models currently available in the literature usually rely on simplifying assumptions and necessitate specific measurements in order to, for example, evaluate the evolution of the coherence length with frequency. This paper describes the work done in order to propose a semi-empirical model for the wall pressure field beneath a fully turbulent boundary layer flow. The main goal is to try to avoid the necessity of preliminary experiments to determine the model coefficients, i.e., propose a model for the power spectral density, coherence length, and phase velocity. After a quick literature review, it proves necessary to acquire a set of experimental data with a fine space–time resolution. Fluctuating wall pressure transducers are developed in this perspective, and experiments are performed in an anechoic wind testing facility. The results are then compared with some published data, analyzed to attempt to offer a schematic description of the physical phenomena involved, and to define the pertinent parameters of the flow and properties of the wall pressure field. These observations are then used to propose a new model for the wall pressure field beneath a fully turbulent boundary layer flow.

1. INTRODUCTION

With increasing flight speed and the generalization of air transportation has appeared a necessity to reduce structural fatigue for vehicles and acoustic and vibration levels for their payload and passengers. More recently, with the increase of train speeds, as well as the considerable improvement of car powertrains and road conditions, this concern has become of great importance for ground transportation, for which interior noise related to the external flow has become a significant noise contributor under certain conditions. As a consequence, since the early 1960s, researchers have been studying the fluctuating loads applied on the structure by the turbulent flow around moving bodies. Concern about such loads first appeared in the aerospace industry, where the shape of the vehicles tends to minimize the regions of flow separation, and the main interest was first focused on attached turbulent boundary layers. However, regions of flow separation are often the main contributors to such loads, with fluctuating levels higher than in the case of

†Present address: Department of Mechanical Engineering, The University of Adelaide, Adelaide, SA 5005, Australia. E-mail: damien.leclercq@adelaide.edu.au.

0022-460X/02/$35.00

attached flows. This is especially true in the automotive industry, where large flow separations are unavoidable on mass-produced cars. In spite of this fact, the present paper also focuses on attached turbulent boundary layers flows, for purposes of simplification in the modelling of the wall pressure field, and the computation of the panel response. Turbulent flow related loads are principally of two types, involving two areas of research.

Firstly, the turbulent fluctuations behave as acoustic sources. The acoustic field resulting from the turbulence then loads the panels which, in turn, transmit noise inside the vehicle. These phenomena are qualified as aeroacoustic. At the low Mach numbers considered here, they become important only in the presence of a protruding accessory that induces strong turbulent stresses in a flow region that consequently behaves as an acoustic source.

Secondly, the interaction between the turbulent flow and the external panels causes wall pressure fluctuations that generate panel vibrations, which radiate sound into the passenger or payload compartment. Feedback from the vibrating panel can also affect the properties of the turbulent flow and its pressure loading.

The discipline of aeroelasticity studies this second type of interaction. However, when trying to predict the body panel responses, the complexity is such that most workers resort to a weak interaction hypothesis, i.e., neglect the panel feedback on the flow. This approach, if valid, i.e., in the absence of aeroelastic instabilities, then allows computation of the panel response from the properties of the wall pressure field experimentally determined on a hard surface.

This paper is concerned with the study and interpretation of the fluctuating wall pressure field generated in the academic case of a fully developed turbulent rigid flat plate boundary layer, for purposes of simplification exposed previously. Choosing the context of the car industry, the present study is focused on the low Mach number and low-frequency domain, for which the so-called aeroelastic phenomena are believed to be predominant, and for which a modal approach can be adopted for a vibrational response computation. However, the plate response is not the subject of this paper.

In order to understand the macroscopic links between the fluctuating flow and the wall pressure, the scientific community have been focusing their work mainly on flat plate turbulent boundary layer flows, as it certainly is the most studied and understood of all basic types of turbulent wall flows. Some studies have also been published on cylinder external flows as well as pipe flows.

Of course, the work done over the last 40 years covers a large variety of Reynolds and Mach numbers. The frequency range of interest also varies greatly from one publication to the next, although most workers intend to examine the widest possible range.

Various types of measurements have been made to characterize the overall pressure fluctuation mean square level, as well as its temporal and spatial evolution. For all the measured data, discrepancies exist even for such basic indicators as the mean square level. These discrepancies have several causes, including different types of transducers used or even the choice of flow variables used to normalize the data. Some published results will be rapidly summarized in the second section of this paper so as to point out and justify the need for yet another set of measurements made with a view to establishing links between the macroscopic flow properties and the wall pressure spectrum features. Section 3 then describes the transducers as well as the experimental set-up used in the present work. The following section describes the measured wall pressure data for purposes of comparison with the literature and interpretation, and the last section formalizes the model that is developed from these experimental observations.

2. WORKING BACKGROUND

Wall pressure time recordings show some typical features that are now well known and agreed upon. They appear to be a random function of space and time with strong fluctuations occurring quite periodically, with a characteristic time that is related to the burst–sweep cycle, an important turbulence-generating phenomenon observed in the inner part of the boundary layer. Haritionidis *et al.* [1] suggested that positive fluctuations are related to sweeps, and more frequent, strong negative fluctuations are the wall signature of bursts. Measuring a signal that is fluctuating in both time and space with a finite size transducer is made difficult because of the spatial averaging that occurs across the sensor surface. For the case of homogeneous fluctuations, Corcos [2] computed a correction function that has proven quite successful provided the sensing area is not too large. Indeed, if some fluctuations are totally averaged out by the transducer surface, it is then impossible to retrieve the lost information with a multiplicative correction function. Schewe [3] underlined the importance of the ratio of transducer diameter to a typical turbulent scale, i.e., that of the burst–sweep cycles. This observation has motivated work to reduce the spatial averaging effect using different types of transducers and mountings. The most obvious way of reducing the sensing area is to cover the transducer with a cap perforated with a small pinhole. The resulting cavity is likely to behave as an acoustic resonator, and it becomes important that the fundamental frequency be as far as possible from the spectral domain of interest. Blake [4] used transducers with a resonance at 17 kHz. Bull and Thomas [5] argued that this type of arrangement induces wall flow perturbations that are measurable on the wall pressure spectrum for frequencies above $0{\cdot}1\,U_\tau^2/2\pi\nu$ with U_τ the friction velocity and ν the kinematic viscosity of the fluid. Quite surprisingly this criterion does not account for the pinhole diameter. Farabee and Casarella [6] whose pinhole measurements are consistent with flush transducer measurement like Schewe's have questioned this conclusion. In most publications, the aim has been to use a transducer with a flat frequency response rather than take the latter into account while processing the recorded data. This has restricted the type of transducer to flush or pinhole mountings of microphones or piezo-electric sensors. Using the transducer's frequency response would allow, as will be seen in the next section, arrangements enabling the measurement of cross-spectra between closer points, such as an offset microphone connected to the surface measurement point by a longer tube. It should also be noted that Lödfahl *et al.* [7] recently developed miniaturized transducers for which a small piezo-resistive element measures the displacement of a 0·4 μm silicone membrane with an active surface as small as a $0{\cdot}01\,\text{mm}^2$. The transducer frequency response is flat within a 6 dB range between 10 Hz and 10 kHz, and its sensitivity is $0{\cdot}9\,\mu\text{V/Pa}$. According to the authors, this arrangement allows measurements of correlations between two points as close as 2 mm. Another interesting and original way of measuring the wall pressure was developed by Emmerling [8], who covered a perforated plate with an elastic reflective foil. The flexible mirrors thus created vibrated under the action of the wall pressure fluctuations and the displacement was measured with interferometry techniques. The technology available at the time made it difficult to process the acquired data. However, the results showed the evolution of the high- and low-pressure zones as they were convected along the surface. One should also mention the use of flexible structures such as membranes [9] or flat plates [10] behaving like filters, selecting from the wall pressure spectrum only some wave numbers corresponding to the considered modes of vibrations.

Of all these techniques, pinhole and flush transducers have been used the most, to obtain results that will now be described. One considers the air (density ρ, dynamic viscosity μ) flowing in the x_1 direction, with a free stream speed U_∞, and a fully developed turbulent

boundary layer of thickness δ defined as $U_1(x_3=\delta)=0{\cdot}99U_\infty$ (U_1 is the mean flow velocity in the x_1 direction), developing on a flat plate that lays in the (x_1,x_2) plane, its leading edge being in $x_1=0$. The outgoing normal to the plate is in the x_3 direction. The displacement thickness δ^*, and the momentum thickness θ of the boundary layer are as defined by Schlichting [11].

In order to predict the vibration spectra of the considered structure, one needs to understand and model the turbulent loads applied on the wall. Such a random fluctuating signal can be described by its power spectral density (PSD) $\phi(\omega)$, $\omega=2\pi f$ with f denoting frequency, as well as its space–frequency evolution, which is necessary to predict how much energy is injected into each mode of the structure.

The overall level of pressure fluctuations $p_{r.m.s.}$ has been measured, generally using two types of normalization: one against the dynamic pressure $q=1/2\rho U_\infty^2$ and another against the wall shear stress $\tau_w=\rho u_\tau^2=\mu\partial U_1/\partial x_{3|_{x_3=0}}$. Both have been extensively used, even if the latter seems more adapted to represent phenomena that take place in the close vicinity of the wall, where the shear stress is an important scaling factor. The relation given by Schlichting [11] between τ_w and q

$$\tau_w = 0{\cdot}0592q\left(\frac{U_\infty x_1}{\nu}\right)^{-1/5} \tag{1}$$

shows that the two representations are far from equivalent. In any case, neither representation yields a constant value from one turbulent boundary layer flow to another. $P_{r.m.s.}/q$ varies between 0·5% and 1% in the various results gathered in reference [3]. When represented against the wall shear stress, the overall level of pressure fluctuation as measured by various authors is represented by Farabee and Casarella [6] with a function computed from the integral over the frequency ranges where the PSD shows, experimentally and theoretically, identified trends:

$$\left(\frac{p_{rms}}{\tau_w}\right)^2 = \begin{cases} 6{\cdot}5, & U_\tau\delta/\nu < 333 \\ 6{\cdot}5 + 1{\cdot}86\ln(U_\tau\delta/333\nu), & U_\tau\delta/\nu > 333 \end{cases}. \tag{2}$$

Blake [4] found a value of 3·6 for $p_{r.m.s.}/\tau_w$, while Schewe [3] extrapolated a value of 2·6 for an idealized transducer of infinitely small area. These different frequency ranges scale on different parameters that are summarized in reference [6]: the lower frequency range $\omega\delta/U_\tau \leqslant 5$ where the power spectrum, driven by the external part of the boundary layer, scales on $q^2\delta^*/U_\infty$, and is a function of $\omega\delta/U_\tau$; the high-frequency range where $\phi(\omega\nu/U_\tau^2)U_\tau^2/\tau_w^2\nu$ is used as a non-dimensional representation; the mid-frequency range, where the PSD scaled as $\phi(\omega\delta/U_\tau)U_\tau/\tau_w^2\delta$ shows its maximum at the dimensionless frequency $\omega\delta/U_\tau \cong 50$. This range also shows the ω^{-1} slope above the maximum, provided the Reynolds number of the flow is high enough. They suggested that the irrotational motions outside the boundary layer also have a strong influence on the wall pressure in the frequency range $30 \leqslant \omega\delta/U_\tau \leqslant 70$, which was confirmed by Wilczynski and Casarella [12]. In fact, both dynamic pressure and wall shear stress determine some part of the spectrum, but equation (2) suggests that the most important parts of the spectrum scale on τ_w.

As for the spatial evolution of the pressure field, its random properties mean that its measurement at one point and a given time can only be made compared to its measured value at another point and another time. The normalized cross-correlation function can be written, in the case of a homogeneous pressure field as

$$R_{pp}(\xi_1,\xi_2,\tau) = \frac{1}{\langle p^2(x_1,x_2)\rangle}\langle p(x_1,x_2,t)p(x_1+\xi_1,x_2+\xi_2,t+\tau)\rangle, \tag{3}$$

where the ensemble averages can be replaced by time averages when the ergodic hypothesis holds. For the case of a fully developed turbulent boundary layer, the streamwise development is slow enough that the wall pressure field can be taken as homogeneous as long as one does not consider too large values for ξ_1. It will be seen that, for large values of the streamwise separation, the signals are no longer related and the correlation function is zero. The wall pressure cross-correlation shows characteristics that are well summarized in the representation made by Willmarth and Wooldridge [13] of their experimental data. For two transducers aligned in the direction of the flow, the cross-correlation shows, when represented against time, a main peak. This peak is centred on the time delay for which the signal measured at the downstream point is the most similar to that measured at the upstream point and time origin. The degree of similarity is given by the height of the peak. It is then possible to compute the broadband convection velocity, as a function of the spatial separation. Taylor's hypothesis, according to which the turbulent flow structures are all preserved as they are convected at the same speed, taken equal to some fraction of the free stream velocity, implies a constant value for the broadband velocity. But this hypothesis, although used by some workers to construct their model [14, 15] is certainly not valid in turbulent shear flows such as boundary layers or jets [16]. In fact, it has been observed that the broadband wall pressure convection velocity increases with longitudinal separation, because the smaller flow structures, closer to the wall where the mean speed is lower, die out more quickly than the larger vortices that lie further away from the wall where the mean speed is higher and the mean shear lower. So, as the distance increases, the wall pressure signal is carried between the two points mostly by the fastest flow structures. The breadth of the cross-correlation peak also increases with ξ_1, because of the loss of the high-frequency fluctuations. This leads to study of the time Fourier transform of the cross-correlation, the cross-spectral density $S_{pp}(\xi_1, \xi_2, \omega)$, so as to analyze the pressure field in the frequency domain.

It is of great interest, for design purposes, to know how the surface features modify the flow and the resulting wall pressure spectra in terms of level and frequency. However, it is far from trivial to determine whether the frequency of the fixed-point wall pressure signal generated by a vortex is determined predominantly by its size or its convection velocity. Working in the space–frequency domain, it is possible to study the signals in view of this equivocal relation between eddy size, convection velocity, and frequency for physical interpretation purposes. It seems that this difficult point has often been overlooked and that the high frequencies have been associated, maybe as a remnant of Taylor's hypothesis, to the small flow structures. This will be further investigated on the measurements presented in the fourth part of this paper.

The cross-spectral density $S_{pp}(\xi_1, \xi_2, \omega)$ can be rewritten by separating the information relative to the power spectrum density $\phi(\omega)$, the coherence $\gamma(\xi_1, \xi_2, \omega)$, and the phase shift $\theta(\xi_1, \xi_2, \omega)$ at any frequency:

$$S_{pp}(\xi_1, \xi_2, \omega) = \phi(\omega)\gamma(\xi_1, \xi_2, \omega)\mathrm{e}^{\mathrm{i}\theta(\xi_1, \xi_2, \omega)}. \tag{4}$$

The rest of this paper aims at understanding, and then modelling these three functions of space and frequency. The space–frequency domain is chosen, rather than the wave number–frequency domain, because it corresponds more closely to the experimental conditions and methods, does not involve a spatial Fourier transform on data that are not finely resolved, and is more adapted to the physical understanding that is expected from these measurements.

3. DESCRIPTION OF THE EXPERIMENTS AND THE WALL PRESSURE TRANSDUCERS

3.1. EXPERIMENTAL SET-UP

Before describing the experimental set up, the necessity for some new experimental data shall be explained. Firstly, it was decided to study the spatial and temporal features of a flow with characteristics similar to those observable on car body external flows in terms of Mach and Reynolds numbers. Experimental data of this type are not the most frequently reported, since the high Reynolds numbers make it difficult to discern the coherent structures in the turbulent flow, or because the measurements were made in conditions simulating high-speed flight. Table 1 summarizes the flow conditions reported in the publications referred to in this paper when they were in the low subsonic range, of interest for the automotive industry. More importantly, authors have generally chosen a mode of representation of their data that precludes the very possibility of trying to define other modes of representation. Separated wall flows, although plentiful on a car, are left aside to concentrate on fully developed turbulent boundary layers for obvious purposes of simplification of the phenomena involved, so as to try and work out the influence of the physical parameters of the flow (such as a boundary layer thickness) on the properties of the wall pressure fluctuations. To further simplify the study, the flow properties should be homogeneous over the considered area. In this view, the measurements must be made at a distance from the boundary layer transition line that is much greater than the streamwise extent of the measurement area, so that the flow properties remain approximately the same at all measurement points.

The purpose of these experiments was two-fold. Firstly, as already stated, it is to understand and establish the properties of the wall pressure fluctuation field: this has then allowed the derivation of a model with physical parameters as inputs, and the least possible arbitrary adjusting constants. The model then gains in generality, so as to be adapted to other cases of flat plate fully developed turbulent boundary layer. Secondly, the structural response of a cavity-backed flexible panel was studied under the same flow conditions and the spectra obtained used to evaluate the response computation based on the wall pressure spectra model developed in the first part of the experiment. This second objective is not developed further here. In this perspective, all the measurements were made below 3000 Hz, where turbulent wall flow loads are believed to generate considerable vibration levels on the car panels at high speeds and where it is possible to study in detail the physics involved in the energy transfers between the turbulent flow and the structure.

The majority of publications describe wind tunnel measurements that are often polluted by the acoustic modes that are established in the wind tunnel, exhibiting strong pressure

TABLE 1

Flow parameters reported in some published works

Reference	U_∞ (m/s)	δ (mm)	δ^* (mm)	θ (cm)	Re_θ
Schewe [3]	6·3	30	4·6	3·3	1400
Blake [4]	22·3–50	42·4–45·7	7·1–7·8	5·7–5·8	8210–17000
Bull and Thomas [5]	24	45·7	5·7	4·57	7000
Farabee and Casarella [6]	15·5–28·3	27·8–27·9	4·3–4·5		3386–6025
Lödfahl *et al.* [7]	30	24	3·8		5072
Wilczynski and Casarella [12]	15·5				3000
Willmarth and Wooldridge [13]	47·6	114	11·6	10·4	29000
Present work	30–40	30·5–28·8	3·8–3·6	3·0–2·8	6480–8160

peaks at low frequencies. Most authors then attempt to remove this acoustic contamination with some signal processing tools, using reference microphones near the acoustic sources to remove the signal components that are coherent with these reference microphones. This relatively simple technique is generally adequate when measuring the wall pressure only. However, as the intention is to measure the response of a cavity-backed panel, acoustic contamination must be rigourously avoided. This necessitates the use of free field conditions, as in the experiments of Hodgson [17] and Efimtsov [18], who made in-flight measurements on a glider wing and a aircraft fuselage panel respectively. However, controlling precisely the flow conditions and obtaining a zero pressure gradient flat plate boundary layer flow on such surfaces seems especially arduous. The test facility that responds to the expressed needs and constraints could thus be a laminar jet blowing in a large anechoic chamber, like CEPRA 19, an open-circuit facility owned at the time by the Office National d'Etudes et de Recherches Aérospatiales, and the Centre d'Essais des Propulseurs in France. It has a 2 m wide circular jet that blows into a large anechoic room, where the air is originally at rest. The available test volume is the 10·84 m long potential cone of the jet, in which the flat plate arrangement must be positioned. Two likely sources of noise are then the mixing layer of the jet, and more importantly at low Mach numbers, its interaction with the hard surfaces of the model support and the resulting dipole type of sound radiation [19]. This possible contamination is monitored closely with reference $\frac{1}{2}''$ microphones in the far field as well as on the flat plate, flush with its surface. The $\frac{1}{2}''$ diameter sensors are meant to average out the smaller scale components of the turbulent signal and measure the longer wavelength acoustic signal. If the acoustic pollution is not detected with this transducer, then it certainly does not affect the turbulent wall pressure measurements made on transducers with a sensing diameter 25·4 times smaller. Coherence levels lower than 0·02 are measured between the wall pressure half inch flush transducers and the farfield microphones for frequencies above 30 Hz.

The model is designed to create a fully developed flat plate turbulent boundary layer. The flow develops on a 15 mm thick aluminium rectangular flat plate, 2·4 m long and 0·9 m wide, that fits in the potential core of the flow. To prevent any extraneous noise generation, the plate is inserted in a 0·3 m thick profiled body. This thickness leaves enough space to fit the cavity for subsequent acoustic measurements. A 0·45 m elliptic leading edge as well as a profiled 1·28 m trailing edge ensure a clean flow on the flat plate. Two semi-circular, cylindrical edges are also added on the sides of the model. The axis of the nozzle is 3·80 m above the ground, and a profiled structure holds the model in position, with the leading edge in the exit plane of the nozzle. Figure 1 presents a side-view diagram of the experimental set-up, where the plate was held vertical in the potential core of the jet. The model was also designed to minimize the risk of mean pressure gradients in the measurement area, in both streamwise and spanwise directions. Static pressure, however, was not measured on the model.

All the metal plates of the ensemble are damped with viscoelastic elements constituted with a thin aluminium plate covered with a bitumen layer and all the empty spaces in the structure are filled with open-cell polyurethane foam blocks.

The wall pressure measurements are made on a 366 mm × 306 mm plate between 1·117 m and 1·483 m downstream of the forced transition. In terms of boundary layer properties, however, the equivalent distance from the transition is longer than the geometrical one, because the thickness of the transition stripe disturbs the flow, and the boundary layer at any point is thickened by this disturbance. For the boundary layer thickness computed from reference [11] to correspond to the measured value, the equivalent distance from the transition is approximately equal to 1·7 m. This means that the boundary layer thickness and friction coefficient, functions of the 4/5th and of the

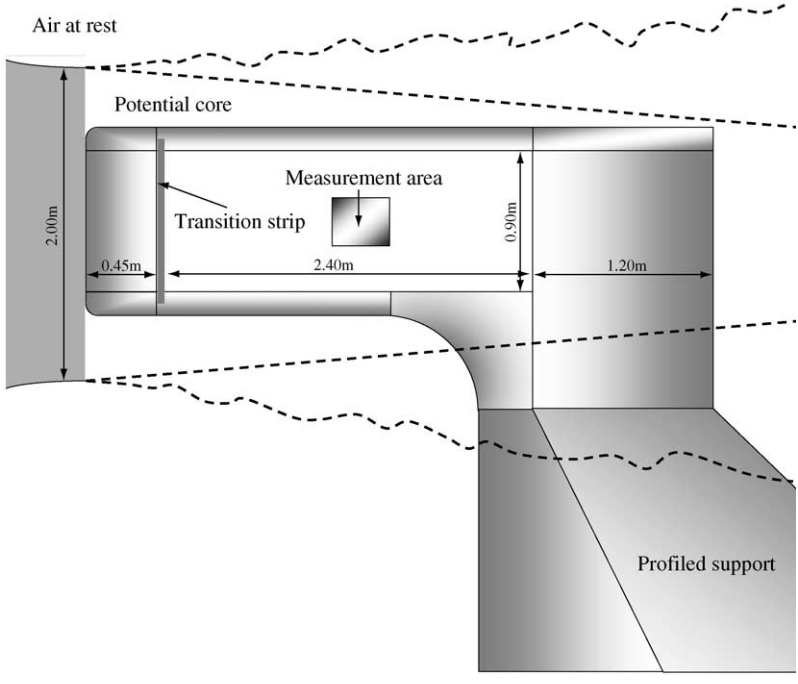

Figure 1. Diagram of the experimental set-up.

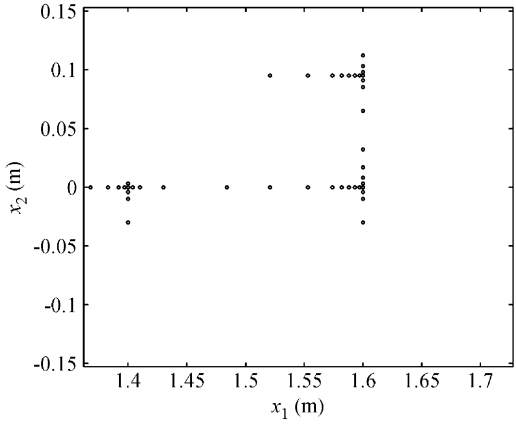

Figure 2. Sketch showing the locations of the 42 wall pressure transducers on the measurement plate.

1/5th power of Reynolds number Re_x based on the distance from the transition, evolve within ± 8 and $\pm 1\%$ of their central value respectively. The root mean square values of the wall pressure signals were within 10% of their mean value, and the spectra were similar, indicating that, for the present purpose, the flow properties can be considered homogeneous all over the measurement area.

The measurement area is equipped with 42 wall pressure transducers with their positions shown in Figure 2, which monitor the evolution of the wall pressure characteristics,

especially homogeneity, across the surface. If homogeneity is guaranteed, it is then possible to use the 861 transducer pairs to map the cross-spectrum with as many points in the first quadrant of the (ξ_1,ξ_2) plane, at any given frequency. Otherwise, the cross-spectrum for a given (ξ_1,ξ_2) varies according to the position of the chosen reference transducer and can only be represented with 41 points, and for each reference position. The number of transducers required makes it necessary to develop and construct sensors that are reliable in the desired frequency range, readily available and inexpensive. These wall pressure transducers are described in the next section. To conclude the description of this experimental set-up, it is important to note that the flow properties were not determined to comply with the spatial averaging criteria, but in view of the computation of the vibrational response of a flat plate that is meant to represent a typical car panel, both in mechanical properties and dimensions. The spatial matching between the plate flexural waves and the wall pressure loading determines the structural response, and this precludes the use of similarities to run the experiments at lower Reynolds number where the wall pressure measurements would be made easier.

3.2. DESCRIPTION AND ASSESSMENT OF THE WALL PRESSURE TRANSDUCERS

This study is focused on rather low frequencies, $30\,\text{Hz} < f < 3000\,\text{Hz}$, where the wall pressure turbulent loading is believed to be an important source of noise in the passenger compartment.

Due to the amount of transducers needed, it was necessary to develop some transducers whose frequency response, even if not flat, was stable enough so that the measured wall pressure spectra could be corrected during the processing of the recordings.

The design that was chosen was a microphone connected to the surface measurement point via a pneumatic connection. The pressure fluctuations that occur at the surface propagate through this capillary tube, and reach the microphone that measures it. However, care has to be taken to avoid strong acoustic resonance which may occur between these boundary conditions, imposed by the free field at the measurement point, and the membrane and cavity on the transducer end. A 3 m long tube, 1 mm in diameter, was chosen so that pressure waves were too attenuated to be reflected at the end of it. A small hole was then drilled in the wall of the tube, at about 32 mm from the measurement point. An Electret microphone capsule glued on the tube measures the pressure through this hole. Such a solution, represented in its final design in Figure 3, makes it possible to

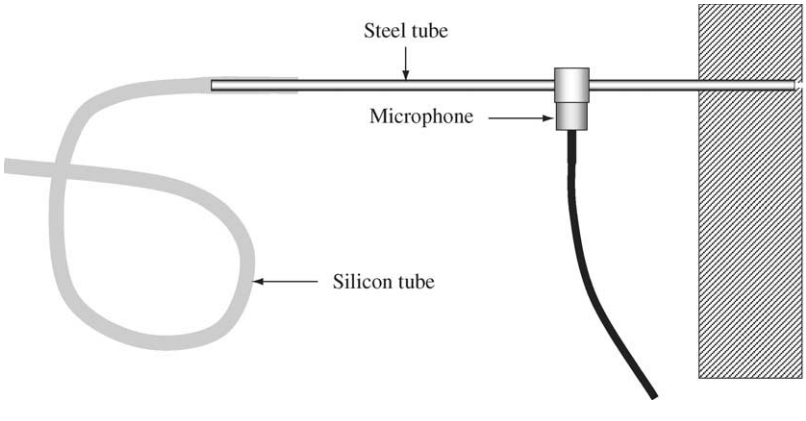

Figure 3. Sketch of the pressure transducers and their mounting on the wall. The hole on the surface has a diameter of 0.5 mm.

measure the pressure at two very close points. To minimize the spatial averaging effect mentioned earlier, the transducers were mounted on the 15 mm thick wall as illustrated in the figure. The transducer tube was positioned behind a hole of small diameter (0·5 mm), 1 mm deep. Assuming a turbulence convection velocity of $0{\cdot}8U_\infty$, the sensing diameter of 0·5 mm sets the Corcos cut-off frequency at 4·8 kHz in the least favourable case considered here, with $U_\infty = 30$ m/s. The rest of the plate thickness was used to maintain the transducer in its position. On the back of the plate, the perimeter of the hole was sealed to prevent any leakage. At 40 m/s, the limit of measurement validity defined in reference [5] would reject frequencies above roughly 2500 Hz.This criterion, however, remains a subject of controversy [6, 20].

Note that this design is an improvement over those that put the transducer at the end of the tube, which is very likely to generate strong resonances that are difficult to attenuate. Gabard [21] has done an extensive work on such transducers. As for the design chosen for this work, Franzoni and Elliott [22] have published a study with various arrangements to improve the anechoicity of this type of transducers. Note also that the 4182 type transducers designed by Brüel and Kjaer have the aspect of the former design, but work rather like the latter.

The coherence measured between two points is insensitive to the transducer response characteristics, but the amplitude and phase of the spectra are. The transducers induce distortions that have to be corrected during the processing of the measured data. Their frequency response function (FRF) thus has to be characterized in a calibration tube with a cut-off frequency of 10 kHz, much higher than the explored frequency range. Note also that, during this FRF measurement, the pinhole mounting of the transducer remains the same as on the measuring plate. The positioning of the transducer relative to the membrane of the reference microphone ensures that the acoustic pressure is the same at both points.

To preclude the possibility of very low-frequency wall pressure fluctuations using all the dynamic range of the acquisition system, all the channels were equipped with A-weighting filters that were used during the flow measurements. This filtering also had to be used during the transducer calibration. A typical frequency response function obtained with these transducers is shown in Figure 4. The frequencies below 1000 Hz are mostly affected by the A-weighting filter, and, between 1 and 4 kHz, the FRF amplitude remains flat within a 2 dB range, while its phase corresponds closely to the acoustic propagation time in the capillary tube between the measuring point and the transducer pinhole in the wall of

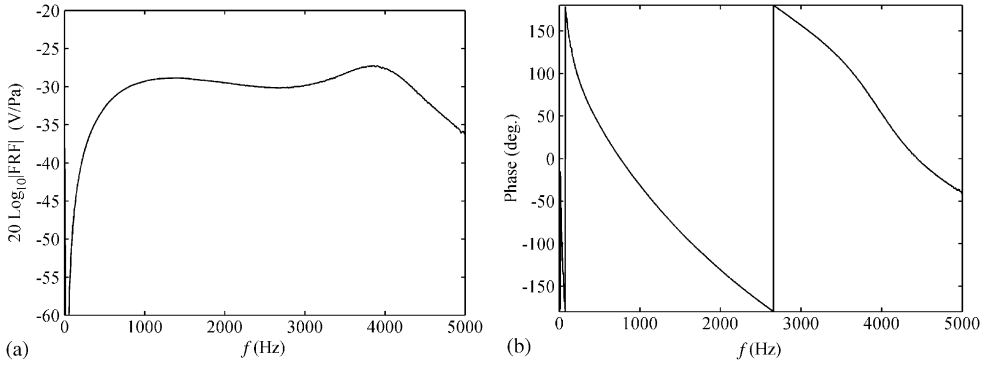

Figure 4. Typical A-weighted frequency response function (FRF) of the pressure transducers developed for the present work: (a) amplitude, (b) phase.

the tube. Note also that the hump just below 4 kHz corresponds roughly to a weak acoustic resonance established on the same section of the tube. Shortening this section increases the resonance frequency, but also makes its amplitude more severe. Besides, this part of the transducer must be long enough, to allow measurements between closely grouped points. The length of this section was kept constant. Measurements thus have to be corrected by the transducer response function, measured in conditions that can differ slightly from the actual wind tunnel ones. Transducers' FRF were measured before and after the wind tunnel measurements were performed. They showed variations of less than 0·5 dB. The error made on the phase velocity estimation is now studied. This variation can result from a difference between the conditions of transducer FRF measurement and those of the wall pressure measurement.

During the transducer frequency response measurement, the phase θ is dominated by the effects of wave propagation in the tube at the velocity c_p over the distance L between the surface point and the microphone: $\theta = \omega L/c_p$. From reference [23], it can be deduced that the sound propagation speed in the capillary tube can be safely approximated by the sound speed in free space. The phase error of the transducer between the calibration conditions and the measurement conditions is then related to variations of L and the sound speed

$$\frac{\Delta\theta}{\theta} \leqslant \left|\frac{\Delta L}{L}\right| + \left|\frac{\Delta c}{c}\right| = \left|\frac{\Delta L}{L}\right| + \frac{1}{2}\left|\frac{\Delta T}{T}\right|, \tag{5a}$$

where T is the absolute temperature. During the flow measurement conditions, the error made on the estimated phase velocity is

$$\frac{\Delta U_p}{U_p} = \frac{\Delta\theta U_p}{\omega L} = \left(\frac{\Delta L}{L} + \frac{1}{2}\frac{\Delta T}{T}\right)\frac{U_p}{c}. \tag{5b}$$

Between the calibration and the measurement, the variation of L is non-negligible only when a flexible tube is used to connect the transducer to the wall. It is not the case in the presented measurements, and the relative measurement error made on the phase velocity reduces to

$$\frac{\Delta U_p}{U_p} = \frac{1}{2}\frac{\Delta T}{T}\frac{U_p}{c}. \tag{5c}$$

Noteworthy is the fact that the relative measurement error is proportional to the phase Mach number U_p/C, which is in the present case much smaller than unity. Hence, with temperature variations that do not exceed 10 K, i.e., approximately 3·5% of the ambient temperature, and a convection velocity of less than the free stream velocity 40 m/s, the error made on the convection velocity by the transducer is then smaller than 0·2%. This error, related to the measurement conditions and the convection Mach number is, of course, negligible when compared to that induced by the loss of coherence of turbulent pressure between the considered transducers. This loss of coherence increases with frequency and transducer separation, and will be further studied in the course of this paper.

4. EXPERIMENTAL RESULTS

Three different boundary layer flows are considered in this paper, at the same abscissa downstream of the forced transition, at 30, 35, and 40 m/s. In the experimental conditions, from the formulae derived in reference [11], one can expect, for the boundary layer thicknesses and the wall shear speed, the approximate values reported in Table 2. The

TABLE 2

Flow data estimated from reference [11] *for three different free stream speeds*

U_∞ (m/s)	δ (mm)	δ^* (mm)	θ (mm)	U_τ (m/s)	$d_c U_\tau / \nu$	d_c/θ
30	30·5	3·8	3·0	1·13	41	0·17
35	29·6	3·7	2·9	1·31	47	0·17
40	28·8	3·6	2·8	1·47	53	0·18

Note: d_c is the transducer diameter. Note that the temperature may vary from one flow speed to the other.

TABLE 3

Overall wall pressure r.m.s. values measured, integrated, between 30 *and* 3000 *Hz for three different free stream speeds*

U_∞	30 m/s	35 m/s	40 m/s
$P_{r.m.s.}/\tau_w$	2·62	2·50	2·44
$100\ p_{r.m.s.}/q$	0·67	0·61	0·57

predicted values of δ are roughly confirmed by hot wire measurements. With this arrangement, wall pressure fluctuations were measured during approximately 3 min, with a sampling frequency of 12·50 kHz. The spectra were computed over 8192 time samples, with a 50% window overlapping, thus allowing approximately 370 averages. As a result, 4096 point spectra were obtained between 0 and 6·25 kHz, with a 5 kHz upper limit imposed by the anti-aliasing filter.

4.1. WALL PRESSURE RMS FLUCTUATIONS

Table 3 presents the values of the root mean square (r.m.s.) pressure fluctuation levels, integrated between 30 and 3000 Hz, and normalized by the wall shear τ_w. The values obtained are in good agreement with those found in the literature (see, e.g., reference [24]), but still decrease with increasing free stream speed. The wall shear is too local a parameter to take the turbulent activity in the whole boundary layer into account, especially regarding the relatively low-frequency range examined here. Similarly, a global parameter, such as the dynamic pressure $q = \rho U_\infty^2/2$, gives results that are also in agreement with the literature if one considers the relatively narrow band of integration of the wall pressure spectrum, but is not adapted to normalize the r.m.s. level. The different frequency ranges reported in reference [6] need to be taken into account.

4.2. WALL PRESSURE POWER SPECTRAL DENSITY (PSD)

Typical spectra obtained are presented in Figure 5 for free stream velocities of 30, 35, and 40 m/s. Using the normalization proposed by Farabee and Casarella [6] for the mid-frequency range, the spectra superimpose very well, indicating that $p_{r.m.s.}/\tau_w$ remains constant when integrated over the frequency range where this normalization holds. Integration over $10 < \omega\delta/\tau_w < 600$ yields a constant value of 2·4 at all three speeds. This value is lower than that suggested by Schewe [3], because the low- and high-frequency

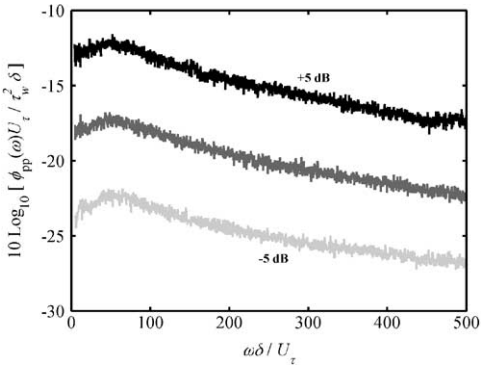

Figure 5. Wall pressure PSD as measured under a turbulent boundary layer at three different free stream speeds. For clarity, the spectra measured at 30 and 40 m/s are shifted by −5 and +5 dB respectively: ——, $U_\infty = 30$ m/s; ——, $U_\infty = 35$ m/s; ——, $U_\infty = 40$ m/s.

TABLE 4

Characteristic frequencies of the wall pressure PSD *maxima at three free stream speeds*

U_∞ (m/s)	30 m/s	35 m/s	40 m/s
$\omega\delta/U_\tau$	49	50	49
$\omega\delta^*/U_\infty$	0·23	0·23	0·23
$\omega\nu/U_\tau^2$	0·020	0·018	0·016

ranges are not taken into account. The available frequency range shows three different zones: a low-frequency positive slope, a rounded peak, and a higher frequency negative slope. As the speed increases, the level increases roughly evenly over the whole frequency range and the frequency of the maximum increases as well. In their dimensionless form, the spectra superimpose very well, and are represented with shifts of +5 and −5 dB for the measurements at 40 and 30 m/s, respectively for purposes of clarity. The former observation seems obvious from the increase of energy in the flow, and the latter can be explained by a higher convection velocity of the turbulent structures containing the most energy, their smaller characteristic size, or both. To understand this dependence, the peak frequency is represented as a Strouhal number based on a characteristic length and speed or in terms of wall units in Table 4.

The use of δ and U_τ shows excellent agreement with the experimental observation in reference [6] that $\omega\delta/U_\tau = 50$ at the maximum of the spectral density. The use of the free stream velocity and the displacement thickness yields values that remain approximately constant when the flow speed varies. The use of wall units does not permit any conclusion. Blake [25] predicts a maximum in the spectrum near $\omega\delta^*/U_\infty$ from 0·2 to 0·3. From reference [11], it is seen that δ and δ* are proportional, and that U_τ is proportional to $U_\infty^{9/10}$. It is thus difficult to decide whether the speed to be considered here is the free stream speed or the friction velocity. Having found that the conclusion drawn in reference [6] is also true in the present case, it will be assumed that the centre frequency of the most energetic part of the wall pressure spectrum is proportional to the friction velocity and the inverse of the boundary layer thickness. On either side of the peak frequency, it is possible to approximate the PSD with power laws $\phi(\omega) \propto \omega^{\alpha i}$. A first positive value α_1 is found at low frequencies below the peak, and two negative slopes α_2 and α_3 are found above the

TABLE 5

Slope coefficients found on the wall pressure PSD *when they are represented as power laws on three different frequency intervals*

U_∞ (m/s)	α_1	α_2	α_3
30	0·22	−0·55	−0·95
35	0·21	−0·57	−0·93
40	0·20	−0·58	−1·07

peak, the steepest one being at frequencies above $\omega\delta/U_\tau \cong 300$. The values found for the α_i are reported in Table 5. They appear to be roughly independent of the flow speed. The frequency range explored here is relatively narrow compared to other published measurements, it is therefore not possible to observe the theoretically predicted (from the Kraichnan Phillips theorem) ω^2 slope at very low frequencies, or the ω^{-5} law at higher frequencies associated with the viscous sublayer activity [25]. It is to be noted, however, that the ω^2 law has been rarely observed by the experimenters (see, for example, reference [6]). The presence of a ω^{-1} evolution, associated with the turbulent activity in the logarithmic layer [26], can be noted. The $\omega^{-0·6}$ slope is less steep than the $\omega^{-0·72}$ and $\omega^{-0·75}$ observed by Hodgson [17], and by Blake [4], respectively, for $\omega\delta^*/U_\infty$ between 0·4 and 0·8. No publication relating the $\omega^{0·2}$ law below the peak has been found.

Having described the spectral energy density of the wall pressure signal, its spatial evolution at each frequency can now be characterized, with the coherence and phase velocity deduced from the cross-spectrum between two points separated by a distance ξ_1 in the streamwise direction and ξ_2 in the spanwise direction.

4.3. WALL PRESSURE COHERENCE

Since the work of Corcos [2], the coherence has frequently been assumed to be a decreasing function of a Strouhal number based on the transducer separation ξ_i, the frequency and a characteristic velocity. This function has in the vast majority of cases been taken as an exponential. However, to describe the fact that coherence does not tend to unity as the frequency tends to zero, Bull [24] distinguished two different behaviours: at sufficiently low frequencies, the coherence is independent of frequency, whereas at higher frequencies, it depends on the Strouhal number based on the phase velocity $U_p(\omega)$, i.e., the phase of the cross-spectrum. Bull found this change to occur about an average value of $\omega\delta^*/U_p(\omega) \cong 0·36$. Corcos also assumed that the loss of coherence between two points separated by (ξ_1, ξ_2) is equal to the loss of coherence in the streamwise direction multiplied by the loss of coherence in the spanwise direction

$$\gamma(\xi_1, \xi_2, \omega) \propto \mathrm{e}^{-\alpha_1\omega|\xi_1|/U_p}\mathrm{e}^{-\alpha_2\omega|\xi_2|/U_p}, \tag{6}$$

where the α_i now denote the loss of coherence in the longitudinal and transverse directions. Bull's results tend to confirm this hypothesis. The validity of this assumption shall be discussed based on the present experiments as well as other published works. This model relies on the concept of a coherence length scale l_n, where $l_n = U_p/\alpha_n\omega$, $n = 1, 2$.

The coherence between two points aligned in the streamwise direction is now considered. Figure 6 shows typical features quickly summarized here. For frequencies above a certain threshold, the coherence between two points decreases with increasing distance and frequency. Below this threshold, the coherence is weaker as the frequency

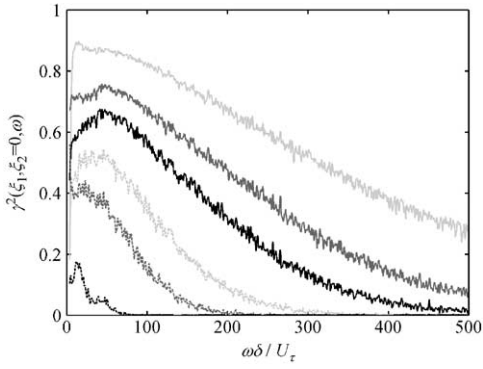

Figure 6. Coherence measured between two transducers with various longitudinal separations ξ_1 ($\xi_2 = 0$, $U_\infty = 40$ m/s): ——, $\xi_1 = 0{\cdot}10\delta$; ——, $\xi_1 = 0{\cdot}24\delta$; ——, $\xi_1 = 0{\cdot}42\delta$; – – – –, $\xi_1 = 0{\cdot}90\delta$; – · – · –, $\xi_1 = 1{\cdot}63\delta$; – – – –, $\xi_1 = 6{\cdot}94\delta$.

decreases. These observations, although slightly different from the description made in reference [24], are consistent with reference [6].

The loss of coherence at high frequencies shows that the turbulent structures generating the high-frequency pressure fluctuations are rapidly destroyed as they are convected. They are either close to the wall, very small and rapidly distorted by the strong shear, or further away from the wall and very small and short lived.

At low frequencies, the structures are either very slow or very large, or both. Slow structures do not last for long enough to convey the pressure information very far. Large structures are rapidly destroyed by the boundary layer shear. Thus, the coherence has a maximum value at a frequency that depends on the distance. For small separations ($\xi_1 \cong \delta^*$), this frequency corresponds roughly to the frequency of maximum energy in the wall pressure spectral density. When distance increases, the threshold frequency decreases. Note also that for small separations, the coherence does not decrease at low frequencies and remains constant for a 3 mm separation, in accordance with reference [24]. This suggests that the coherence tends to unity only when ξ_1, and not ω, diminishes. This goes against the use of the dimensionless number $\omega\xi_1/U_p(\xi_1, \omega)$ in this range. Also noteworthy is the fact that the coherence remains non negligible at low frequencies for very large distance. This is the pressure signature of irrotational motions outside the boundary layer, caused by the action of the irregular boundary layer edge of the intermittency zone on the free stream, as described in reference [12]. Using an exponential function of the phase of the cross-spectrum, $\omega\xi_1/U_p(\omega)$ has become the common way of representing the data. However, the comparisons are, in the literature as with the present data, not very satisfying and there is no definite value for α_1. Even if it is possible to obtain an exponential function that roughly approximates the data, much like an envelope, there is no real agreement between the coherence functions and the proposed model: as an illustration, one reference point is chosen and the coherence with four other transducers, aligned in the direction of the flow, at various distances ξ_1 from the reference, is computed. The value of α_1 is then estimated from equation (6), and Figure 7 shows the values obtained at all frequencies. The value of α_1 varies greatly with frequency and spatial separation for normalized frequencies lower than 100, thus invalidating the use of a coherence length scale at low frequencies, where the boundary layer thickness determines the largest possible length scales. At higher frequencies, ξ_1 increases steadily with frequency and varies little with ξ_1, thus confirming the exponential decay with regard to spatial separation, and validating the use of a coherence length scale, a function of the

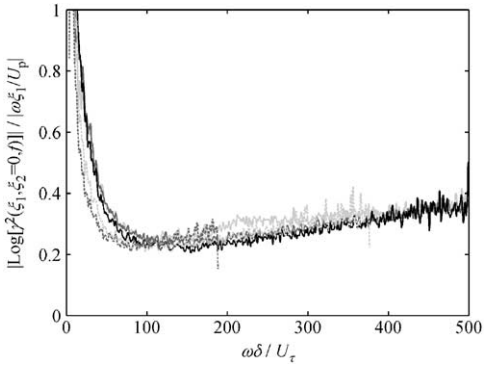

Figure 7. Coherence decay rate α_1 measured between two transducers with various longitudinal separations ξ_1 ($\xi_2 = 0$, $U_\infty = 40$ m/s): ——, $\xi_1 = 0{\cdot}10\delta$; ——, $\xi_1 = 0{\cdot}24\delta$; ——, $\xi_1 = 0{\cdot}42\delta$; (smoothed data); – – – –, $\xi_1 = 0{\cdot}90\delta$; – · – · –, $\xi_1 = 1{\cdot}63\delta$.

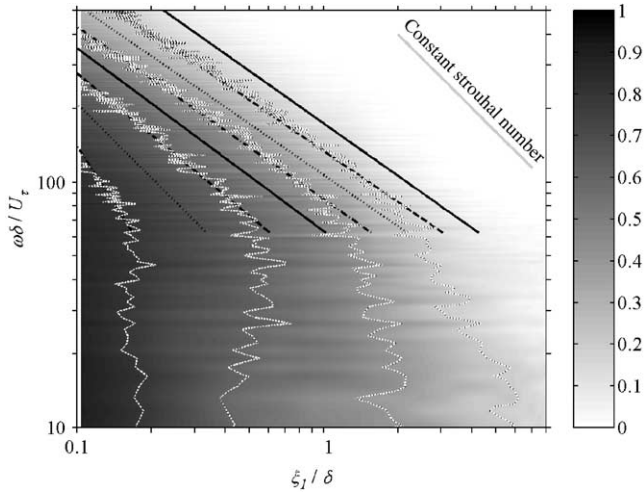

Figure 8. Streamwise coherence represented as a function of the longitudinal separation and the frequency ($U_\infty = 40$ m/s). The level of coherence is represented by the grey level. Some level lines are also represented for 0·2, 0·4, 0·6, and 0·8. Above 500 Hz, these curves are approximated by straight lines that are the geometric representation of γ^2 ($f^n\xi_1$, $\eta = 0$) = constant, where n is determined from the measurements. Smoothed data.

frequency. In any case, α_1 shows no tendency to remain constant, and it becomes obvious that its variation with frequency needs to be taken into account, as often reported in the literature. It should be noted that U_τ was used to scale the frequency in Figure 7, instead of $U_p(\omega)$, used in the literature. However, the use of the phase velocity in the coherence model means that it has to be modelled as well, or replaced by a constant velocity, e.g., U_∞, with its frequency dependence taken into the $\alpha_1(\omega)$ function. Furthermore, as will be seen in the next section, the phase velocity also varies with ξ_1. Hence, not finding any simple dimensionless number against which coherence can be plotted, the latter is mapped in the (ξ_1/δ, $\omega\delta/U_\tau$) plane, with a logarithmic scale. If the coherence were a function of ($\omega\xi_1/U_\tau$) only, then the curves of constant coherence levels would be, on this graph, straight lines of slope -1. With use of a Matlab routine that extracts the lines of constant level as well as their slope, Figure 8 presents the original coherence function, its level lines, and their straight-line approximation at dimensionless frequencies above 60. It is firstly obvious that

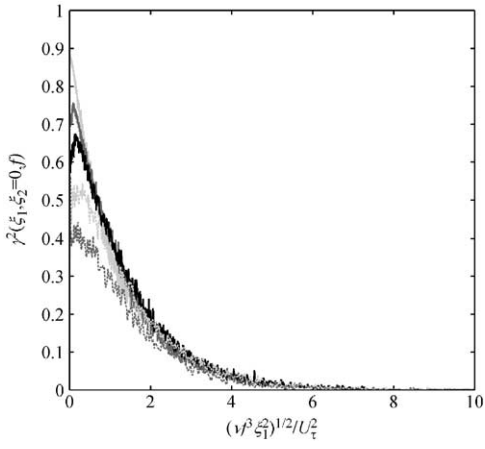

Figure 9. Streamwise coherence as a function of the dimensionless number $(vf^3\xi_1^2)^{1/2}/U_\tau^2$, $U_\infty = 40$ m/s: ——, $\xi_1 = 0{\cdot}10\delta$; ——, $\xi_1 = 0{\cdot}24\delta$; ——, $\xi_1 = 0{\cdot}42\delta$; – – – –, $\xi_1 = 0{\cdot}90\delta$; – · – · –, $\xi_1 = 1{\cdot}63\delta$.

the constant level lines are not parallel to the constant Strouhal line also represented. In fact, the coefficients found tend to indicate, above approximately 500 Hz ($\omega\delta/U_\tau > 60$), that the coherence is a function of a number based on $f^{3/2}|\xi_1|$. A dimensionless number can then be constructed, and it is meant to determine the evolution of the coherence. The fluid kinematic viscosity v as well as the wall friction velocity U_τ are chosen as the most important quantities that affect the observed phenomena. Upon assuming that the fluid viscosity destroys the coherent flow structures, and that the increase in wall friction velocity improves their preservation as they are convected, the following dimensionless number is obtained after dimensional analysis $\sqrt{vf^3\xi_1^2}/U_\tau^2$. Figure 9 shows that the decreasing part of the coherence functions superimpose quite well on a decreasing exponential when represented against this dimensionless number. At low frequencies however, the coherence remains well below unity. This limitation can be associated to the boundary layer thickness and the friction velocity that limit the size and life span of large structures.

4.4. WALL PRESSURE PHASE SPEED

4.4.1. *Frequency analysis*

As a preliminary to the subsequent observations, it is important to note that it is not clear whether the frequency of the pressure fluctuations generated by coherent structures is determined by their scale or their convection velocity. In that sense, Taylor's frozen pattern convection hypothesis has been frequently used to interpret the experimental data: the whole turbulent flow is assumed to be convected at a uniform speed and the frequency of the velocity fluctuations is directly proportional to the convection velocity and the inverse of the turbulent scale. This hypothesis enables the peaks in the wave number–frequency spectra to be located correctly, but it does not apply with turbulent shear flows where the mean velocity varies notably across the flow, thus affecting the shape of the pressure peak. The picture is further complicated by the fact that the turbulent scales are also determined by the mean shear. Thus, in a boundary layer, small structures are dominant close to the wall where the mean speed is also slow. Do these structures contribute to the relatively low or high frequencies? The issue is of importance when the

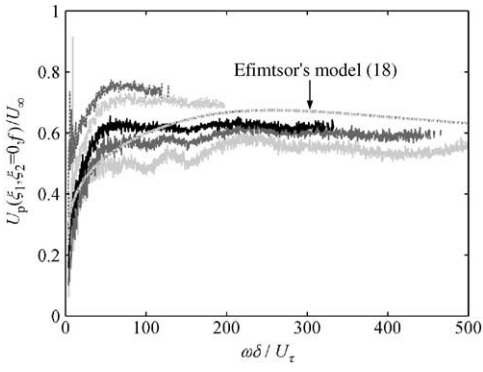

Figure 10. Streamwise phase velocity ($U_\infty = 40$ m/s). Smoothed data: ——, $\xi_1 = 0{\cdot}10\delta$; ——, $\xi_1 = 0{\cdot}24\delta$; ——, $\xi_1 = 0{\cdot}42\delta$; – – – –, $\xi_1 = 0{\cdot}90\delta$; – – – –, $\xi_1 = 1{\cdot}63\delta$.

velocity profile at the wall can be affected in order to modify the fluctuating wall pressure field, and the following discussion is an attempt to relate the turbulent flow structures to the wall pressure in the frequency domain, based on wall pressure phase velocity measurements, as well as the coherence measurements reported previously.

Considering the phase speed measured between two transducers aligned in the streamwise direction, the distance ξ_1 between the transducers only selects the ratio of signal generated by the turbulent structures that can travel this far, and that contribute to the coherence. Figure 10 shows the phase velocity against frequency at several transducers separations, along with the model proposed by Efimtsov [18]. This model shows roughly the same trends as the present measurements, except for the fact that it does not take account of the variations with ξ_1. The present results are similar to those reported in reference [6]. At all frequencies, the measured phase speed increases with ξ_1, which means that for a given distance, the coherent structures that do not travel the distance ξ_1 are the slowest. Assuming, without risk, that the convection velocity of turbulent fluctuations is related to the local mean speed, these structures are consequently close to the wall, hence of relatively small scale. This leads one to conclude that small scales play an important role over the whole frequency range explored here, depending on their convection velocity. At low frequencies, the phase speed is low, and the coherence is weak, thus indicating that the pressure fluctuations are generated by small scales near the wall that are too slow to be convected over a distance. As the frequency increases, both phase velocity and coherence increase, and larger, faster structures, further away from the wall start playing an important role. For dimensionless frequencies above 60, the phase velocity remains quite high but decreases slowly, while the coherence decreases more sharply. This can be interpreted as the action of the turbulent structures of all length scales in the outer part of the boundary layer that are convected at similar speeds, while the smallest scales die out more rapidly, thus causing a sharp decrease in the coherence with frequency.

Of course, the phase velocity does not continuously increase with ξ_1 and seems to reach, when $\xi_1 > 4\delta$, an asymptotic value of approximately $0{\cdot}8U_\infty$, which is commonly observed in the published literature. The convection velocity, estimated from broadband cross-correlations, is now studied from a more quantitative point of view.

4.4.2. *Broadband analysis*

The broadband convection velocity U_c is determined from the inverse Fourier transform of the cross-spectra, taken between 50 and 3000 Hz.The cross-correlation functions display

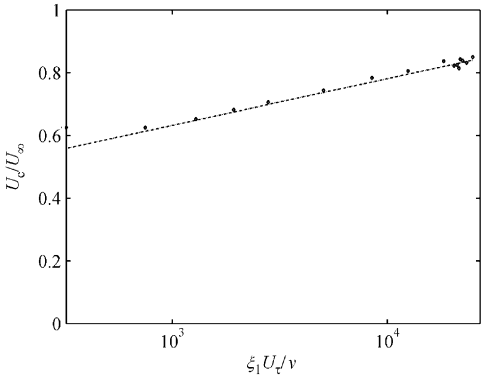

Figure 11. Broadband streamwise convection velocity ($U_\infty = 40$ m/s). Frequency integration is done between 50 and 3000 Hz.

a main peak at a delay that corresponds to the time it takes for the most energetic part of the signal to be convected between the two transducers. The convection velocity deduced from this delay and the transducer separation ξ_1 is plotted in Figure 11. Also represented in the figure is the logarithmic law

$$\frac{U_c(\xi_1)}{U_\tau} = \frac{1}{\kappa_0} \mathrm{Ln} \frac{|\xi_1| U_\tau}{\nu} + C_0, \tag{7}$$

with $\kappa_0 = 0{\cdot}57$ and $C_0 = 5{\cdot}0$ for the 40 m/s boundary layer. This law shows a good agreement with the measured data. Assuming that the boundary layer mean velocity profile follows a logarithmic law, one can deduce that, in the examined range, the dominant contribution for a given transducer separation seems to originate from a layer defined by its distance from the wall related to the transducer separation ξ_1.

5. PROPOSITION OF A MODEL FOR THE WALL PRESSURE SPECTRUM

5.1. WALL PRESSURE PSD

The model proposed for the wall pressure PSD relies on the aforementioned observations: it presents a maximum centred on $\omega\delta/U_\tau \cong 50$, that is represented, in the (Ln(f),Ln(PSD)) plane, by a portion of circle of radius equal to $U_\tau/2\pi\delta$. On either side of this maximum, the model obeys the $f^{0{\cdot}2}$ and $f^{0{\cdot}6}$ laws. Finally, its global level is determined by a value of $p_{r.m.s.} = 2{\cdot}4\tau_w$ when integrated over the frequency range $10 < \omega\delta/\tau_w < 600$. The model is aimed at computing the structural response of a panel with a modal decomposition at low and medium frequencies. Hence, to keep it simple, no account is taken of the -1 slope at higher frequencies. Figure 12 shows the comparison between the model and the experiments at three different speeds: the proposed formulation is a satisfying approximation for the wall pressure PSD.

5.2. WALL PRESSURE COHERENCE

In section 4.3, the lower frequency coherence degradation was associated to the limitation in eddy size imposed by the boundary layer thickness δ, and the destruction of the largest structures by the wall shear. To take this dependence into account, while keeping a simple formulation for the coherence, an exponential function of the

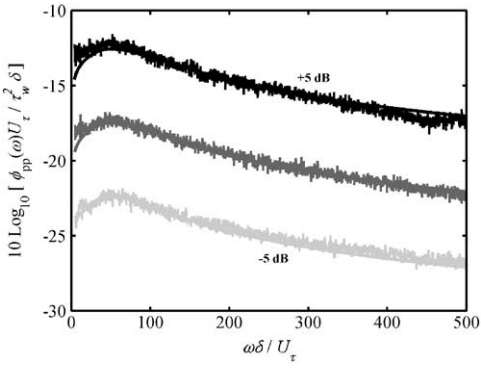

Figure 12. Wall pressure PSD as measured under a turbulent boundary layer at three different free stream speeds, comparison between model and measurements. For clarity, the spectra measured at 30 and 40 m/s are shifted by −5 and +5 dB respectively: ——, $U_\infty = 30$ m/s; ——, $U_\infty = 35$ m/s; ——, $U_\infty = 40$ m/s.

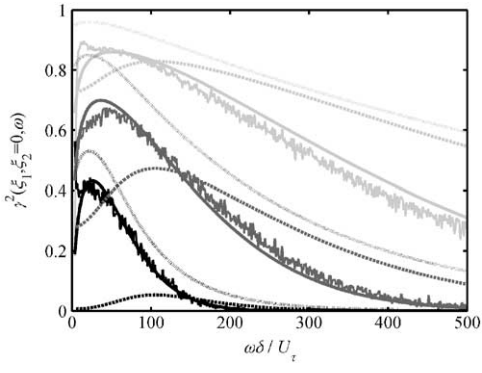

Figure 13. Coherence measured between two transducers with various longitudinal separations ξ_1 ($\xi_2 = 0$, $U_\infty = 40$ m/s), comparison between models and measurements. Proposed model: ——, $\xi_1 = 0{\cdot}10\delta$; ——, $\xi_1 = 0{\cdot}42\delta$; ——, $\xi_1 = 1{\cdot}63\delta$. Efimtsov's model: – – – –, $\xi_1 = 0{\cdot}10\delta$; – – – –, $\xi_1 = 0{\cdot}42\delta$; – – – –, $\xi_1 = 1{\cdot}63\delta$. Smol'yakov and Tkachenko's model: ·····, $\xi_1 = 0{\cdot}10\delta$; ·····, $\xi_1 = 0{\cdot}42\delta$; ·····, $\xi_1 = 1{\cdot}63\delta$.

dimensionless number $-\sqrt{|\xi_1| U_\tau / f\delta_{99}^2}$ is applied as a correction factor. The longitudinal can thus be modelled as

$$\gamma(\xi_1, 0, f) = \mathrm{e}^{-\sqrt{\nu f^3 \alpha_1^2 \xi_1^2}/U_\tau^2}\,\mathrm{e}^{-\sqrt{\sqrt{\beta_1^2 \xi_1^2} U_\tau / f\delta_{99}^2}}, \tag{8}$$

with $\alpha_1 = 0{\cdot}43$ and $\beta_1 = 0{\cdot}25$. Note that outside the low-frequency range where the length scales are limited by the boundary layer thickness, the proposed model relies on the concept of coherence length scale l_1, with $l_1 = U_\tau^2 / \sqrt{\nu f^3 \alpha_n^2}$. Comparison of this model with the experimental data shows, in Figure 13, good agreement at 40 m/s, as well as at the other two flow speeds considered here. The curves predicted by the models of Efimtsov [18] and Smol'yakov and Tkachenko [14] are also added, and overestimate the coherence at high frequencies. At low frequencies, the former model underestimates the coherence, while the latter one overestimates it.

As for the transverse direction, the same type of dependence is assumed, and the coefficients found are $\alpha_2 = 2{\cdot}98$ and $\beta_2 = 5{\cdot}53$. The agreement between the model and the measurements is in this direction less accurate at very low frequencies (Figure 14). The

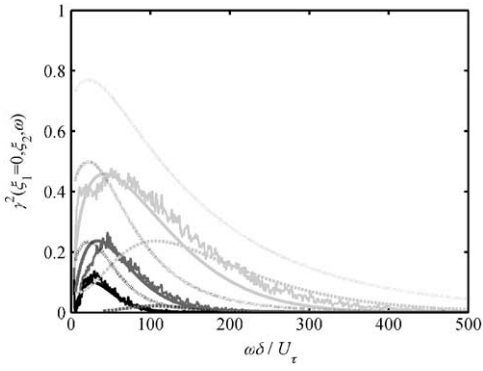

Figure 14. Coherence measured between two transducers with various longitudinal separations ξ_1 ($\xi_2=0$, $U_\infty=40$ m/s), comparison between models and measurements. Proposed model: ——, $\xi_1=0{\cdot}10\delta$; ——, $\xi_1=0{\cdot}28\delta$; ——, $\xi_1=0{\cdot}59\delta$. Efimtsov's model: – – – –, $\xi_1=0{\cdot}10\delta$; – – – –, $\xi_1=0{\cdot}28\delta$; – – – –, $\xi_1=0{\cdot}59\delta$. Smol'yakov and Tkachenko's model: ·····, $\xi_1=0{\cdot}10\delta$; ·····, $\xi_1=0{\cdot}28\delta$; ·····, $\xi_1=0{\cdot}59\delta$.

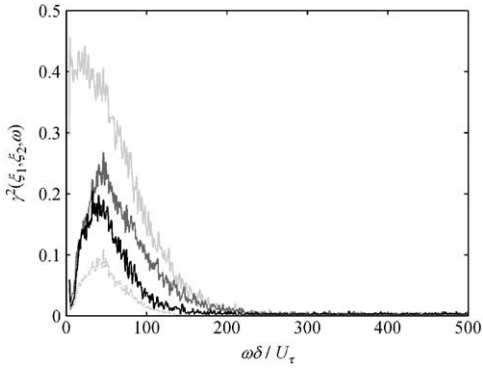

Figure 15. Evaluation of the possibility of modelling the off-axis coherence as a product of longitudinal and transversal coherence functions: ——, $\gamma^2(\xi_1,\ 0,\ f)$; ——, $\gamma^2(0,\ \xi_1,\ f)$; ——, $\gamma^2(\xi_1,\ \xi_2,\ f)$; – – – –, $\gamma^2(\xi_1,0,f)\gamma^2(0,\xi_2,f)$.

predictions based on the models of Efimtsov [18] and Smol'yakov and Tkachenko [14] are further away from the measured coherence.

A model for the off-axis coherence is now needed, i.e., a general shape for coherence surfaces in the (ξ_1,ξ_2) plane is chosen. In this plane, do the lines of constant level of coherence have the shape of diamonds, like with model (6) of Corcos [2], or Efimtsov [18] in his model derived from measurements on a aircraft fuselage panel, or ellipses, as suggested by Singer [27] from his large eddy simulation of a boundary layer flow, and assumed by Smol'yakov and Tkachenko [14] in their model based on a wind tunnel wall measurements? The position of the measurement points allows a representation of the coherence at several points in the (ξ_1,ξ_2) plane at any given frequency, and it is possible to draw some conclusions regarding the shape of the off-axis coherence, even if the surface is still poorly resolved. From the present measurements, the slope of the lines of constant level leads to question the validity of the assumption that the coherence can be the product of two functions—of ξ_1 and ξ_2 respectively. Comparison of $\gamma^2(\xi_1,\xi_2,f)$ and the product $\gamma^2(\xi_1=0,\xi_2,f)\ \gamma^2(\xi_1,\xi_2=0,f)$, shown in Figure 15, is a convincing evidence of the invalidity of this hypothesis in the present case. This figure shows how an elliptic model and a separated space variables model would compare to the off-axis coherence

measurements if these models represented perfectly the streamwise and spanwise coherence. The measurements tend to show that the coherence contours have an elliptic form in the (ξ_1,ξ_2) plane. Hence, the coherence model that is proposed for all frequencies and separations takes the form:

$$\gamma(\xi_1,\xi_2,f) = \mathrm{e}^{-\sqrt{vf^3\left(\alpha_1^2\xi_1^2+\alpha_2^2\xi_2^2\right)}/U_\tau^2}\,\mathrm{e}^{-\sqrt{\sqrt{\left(\beta_1^2\xi_1^2+\beta_2^2\xi_2^2\right)}U_\tau/f\delta_{99}^2}}, \tag{9}$$

with the four constants α_i and β_i previously defined. Note that apart from the very low-frequency limit, this model also uses the concept of length scale in both directions, and presents an exponential decay with $|\xi|$. Expression (9) describes its evolution with frequency in a relatively simple form, with an $f^{-3/2}$ term in the length scale formulation. The coherence model does not rely on the phase velocity, whose variation with frequency and spacing is rather complicated in the present case like in reference [6].

5.3. WALL PRESSURE PHASE VELOCITY

As for the phase velocity, the results obtained are less than clear, and it is difficult to approximate them with a simple model. As a somewhat rough approximation, the phase velocity is assumed to have its maximum value at the same frequency of $2\pi f\delta/U_\tau \cong 50$. Below this maximum, it increases as a function of the dimensionless number $\sqrt{vf^3\xi_1^2/U_\tau^2}$, as a logarithmic law. Above the maximum, it follows a decreasing logarithmic function of the frequency only:

$$U_p = \begin{cases} 0{\cdot}07U_\infty \ln\left(\sqrt{vf^3\xi_1^2}/U_\tau^2\right) + 0{\cdot}78U_\infty, & 2\pi f\delta/U_\tau \leqslant 50 \\ U_{p\,MAX}, & 2\pi f\delta/U_\tau = 50 \\ U_{p\,MAX} - 0{\cdot}7U_\tau \ln(2\pi f\delta/50U_\tau), & 2\pi f\delta/U_\tau > 50 \end{cases}. \tag{10}$$

Some choices made for this model are certainly arbitrary. But, as shown in Figure 16, it represents the measured data more closely than the models currently found in the literature, that do not take into account the dependence on both the frequency and the longitudinal separation distance. As a consequence, in the experimental case considered here, it is expected to yield better results for predictive structural response computations.

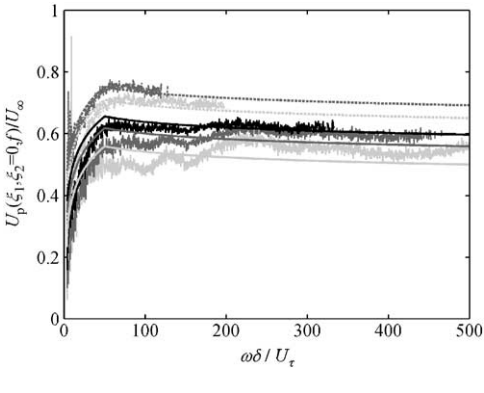

Figure 16. Phase speed measured between two transducers with various longitudinal separations $\xi_1(\xi_2=0,$ $U_\infty=40$ m/s), comparison between models and measurements: ——, $\xi_1=0{\cdot}10\delta$; ——, $\xi_1=0{\cdot}24\delta$; ——, $\xi_1=0{\cdot}42\delta$; – – – –, $\xi_1=0{\cdot}90\delta$; – · – · –, $\xi_1=1{\cdot}63\delta$.

A turbulent wall pressure field model has thus been constructed, based on measurements made beneath three different fully developed turbulent boundary layers. These results allowed the model to avoid the over-simplifying assumptions that seemed too far removed from the experimental results found in the literature as well as those presented here.

6. CONCLUSIONS

Although a general consensus exists about some features of the wall pressure field beneath subsonic flat plate turbulent boundary layers, there are still many characteristics that remain open for interpretation and understanding. Some of them, like the coherence, are modelled as an exponential function of a dimensionless number based on the frequency, the separation distance, and a velocity, chosen as a constant ratio of the free stream velocity or the phase velocity. In these cases it was shown that this type of model shows significant discrepancies with the measurements, in the published literature as in this paper. Furthermore, the use of the phase velocity, although it clearly improves the model, requires the knowledge of this function, whose space–frequency behaviour is poorly understood. As for the phase velocity itself, models rarely take into account its evolution with distance and frequency at the same time. Some models even assume it to be a constant fraction of the free stream speed.

The experimental data acquired here gave the bases to develop a new model, without resorting to the assumptions already made in the literature when they seemed misleading or inaccurate. With a methodical procedure and the help of a fine space–frequency resolution offered by the use of a large number of wall pressure transducers that were developed for this work, the large amount of data measured gave enough material to propose a model that describes the present measurements quite accurately at three different free stream speeds. This model agrees with some conclusions found in the literature, and offers new views on the space–frequency dependence of the wall pressure field, especially regarding coherence and phase velocity. These quantities can be shown to have a strong influence on the modal response of flexible panels [28], especially when the convection velocity is below the hydrodynamic coincidence. The proposed model describes some trends of the wall pressure field that were not taken into account by other models. As a consequence, this proposed model can be hoped to correct some inaccuracies that are observable in the literature with the classical models. However, a full validation necessitates the comparison with data obtained beneath fully turbulent subsonic boundary layers by other experimenters and with different test facilities.

The ultimate goal of such a model is to predict the vibrational response of flexible panels, and the second and final stage of this work will be to see if the claimed improvement shows on the comparison between the measured and the computed structural response. Several publications show indeed a wide range of predicted levels for the same structure and flow conditions, according to which model is chosen [28,29]. In all cases, the computed responses strongly overestimate the experimental results, and the accuracy of the predicted response levels is very sensitive to the space–time characteristics of the turbulent load, i.e., the coherence and phase velocity.

ACKNOWLEDGMENTS

The first author gratefully aknowledges the ''Association Nationale de la Recherche Technique'' for a ''Convention Industrielle de Formation par la Recherche'' grant.

REFERENCES

1. J. G. Haritonidis, L. S. Gresko and K. S. Breuer 1990 in *Near-Wall Turbulence* (J. S. Kline and N. H. Afgan, editors), 397–417. New York: Hemisphere.
2. G. M. Corcos 1963 *Journal of the Acoustical Society of America* **35**, 192–199. Resolution of pressure in turbulence.
3. G. Schewe 1983 *Journal of Fluid Mechanics* **134**, 311–328. On the structure and resolution of wall pressure fluctuations associated with turbulent boundary-layer flow.
4. W. K. Blake 1970 *Journal of Fluid Mechanics* **44**, 637–660. Turbulent boundary-layer wall-pressure fluctuations on smooth and rough wall.
5. M. K. Bull and A. S. W. Thomas 1976 *Physics of Fluids* **19**, 597–599. High frequency wall pressure fluctuations in turbulent boundary layers.
6. T. M. Farabee and M. J. Casarella 1991 *Physics of Fluids A* **3**, 2410–2420. Spectral features of wall pressure fluctuations beneath turbulent boundary layers.
7. L. Lödfahl, E. Kälvesten and G. Stemme 1996 *Journal of Fluid Engineering* **118**, 457–463. Small silicon pressure transducers for space–time correlation measurement in a flat plate boundary layer.
8. R. Emmerling 1973 *Max Plank Institut für Strömungsforschung, Göttingen, Report No.* 9. The instantaneous structure of the wall pressure under a turbulent boundary layer flow.
9. N. C. Martin and P. Leehey 1977 *Journal of Sound and Vibration* **52**, 95–120. Low wavenumber wall pressure measurements using a rectangular membrane as a spatial filter.
10. P. W. Jameson 1975 *Proceedings of the Symposium on Turbulence in Liquids, University of Missouri, Rolla*. Measurement of the low-wavenumber component of turbulent boundary layer pressure spectral density.
11. H. Schlichting 1979 *Boundary Layer Theory*. New York: McGraw-Hill; seventh edition, 636–647.
12. V. Wilczynski and M. J. Casarella 1995 *Transactions of the American Society of Mechanical Engineers* **117**, 252–262. Influences of near-wall and induced irrotational motion in a turbulent boundary layer on wall pressure fluctuations.
13. W. W. Willmarth and C. E. Wooldridge 1962 *Journal of Fluid Mechanics* **14**, 187–210. Measurements of the fluctuating pressure at the wall beneath a thick turbulent boundary layer.
14. A. V. Smol'yakov and V. M. Tkachenko 1991 *Soviet Physics Acoustics* **37**, 627–631. Model of a field of pseudosonic turbulent wall pressures and experimental data.
15. D. M. Chase 1980 *Journal of Sound and Vibration* **70**, 29–67. Modelling the wavevector-frequency spectrum of turbulent boundary layer wall pressure.
16. M. J. Fisher and P. O. A. L. Davies 1965 *Journal of Fluid Mechanics* **18**, 97–116. Correlation measurements in a non frozen pattern of turbulence.
17. T. H. Hodgson 1962 *Ph.D. Thesis, Faculty of Engineering, University of London*. Pressure fluctuations in shear flow turbulence.
18. B. M. Efimtsov 1982 *Soviet Physics Acoustics* **28**, 289–292. Characteristics of the field of turbulent wall pressure fluctuations at large Reynolds numbers.
19. N. Curle 1953 *Proceedings of the Royal Society of London, Series A* **231**, 505–514. The influence of solid boundaries upon aerodynamic sound.
20. M. K. Bull 1996 *Journal of Sound and Vibration* **190**, 299–315. Wall-pressure fluctuations beneath turbulent boundary layers: some reflections on forty years of research.
21. S. Gabard 1994 *Ph.D. Thesis, Centre d'Etudes Aérodynamiques et Thermiques, Université de Poitiers*. Contribution à l'étude de l'influence d'une liaison pneumatique sur la transmission et la mesure des fluctuations de pression.
22. L. P. Franzoni and C. M. Elliott 1998 *Journal of the Acoustical Society of America* **104**, 2903–2910. An innovative design of a probe-tube attachment for a $\frac{1}{2}$-in. microphone.
23. C. Zwikker and C. Kosten 1949 *Sound Absorbing Materials*. Amsterdam: Elsevier.
24. M. K. Bull 1967 *Journal of Fluid Mechanics* **28**, 719–754. Wall pressure fluctuations associated with subsonic turbulent boundary layer flow.
25. W. K. Blake 1986 *Mechanics of Flow Induced Sound and Vibration, Vol. II*. New York: Academic Press Inc.
26. P. Bradshaw 1967 *Journal of Fluid Mechanics* **30**, 241–258. "Inactive" motion and pressure fluctuations in turbulent boundary layers.
27. B. A. Singer 1996 *NASA Contract NAS1*-20059. Turbulent wall pressure fluctuations: new model for off-axis cross spectral density.

28. D. J. J. LECLERCQ 1999 *Ph.D. Thesis, Département Génie Mécanique, Université de Technologie de Compiègne*. Modélisation de la réponse vibro-acoustique d'une structure couplée à une cavité en présence d'un écoulement turbulent.
29. W. R. GRAHAM 1997 *Journal of Sound and Vibration* **206**, 541–656. A comparison of models for the wavenumber–frequency spectrum of turbulent boundary layer pressures.